Scientic Uses of Crude Telemetry during Mars Atmospheric Entry

Dr. Paul Withers (Boston University)

Accurate acceleration measurements during atmospheric entry have long been used to derive atmospheric properties, such as density, pressure, and temperature. How well can **atmospheric properties** be derived from inaccurate velocity measurements via **Doppler-shifted telemetry**?

Such a technique would (a) work even if the spacecraft **splats upon impact** before returning its recorded science data and (b) **work in real time** during the descent, providing instant data for the eager public.

I will present analysis techniques that are optimized to work with inaccurate velocity measurements instead of accurate acceleration measurements. Accelerations derived from repeated inaccurate velocities are very, very uncertain indeed.

Reasonable results for pressure and temperature, but not density, profiles appear possible. A surprisingly accurate measurement of temperature at peak acceleration is also possible.

Abstract 14.24, 35th DPS Meeting, Monterey, CA, 2003.09.03

Motivation

MER will have a **direct-to-Earth telemetry** link during its entry into the martian atmosphere. The Doppler shift in its telemetry is fixed by its line-of-sight velocity. In this poster I use a **simplified entry geometry** to test whether these crude measurements of its speed as a function of time can provide any useful information on **atmospheric density, pressure, and temperature**.

I start with the basic, time-honoured ideas of entry accelerometer data analysis and adapt them to be **suitable for inaccurate velocity**, and even more inaccurately derived acceleration, measurements, rather than accurate acceleration measurements. It is better to use an approximate technique that works with the most accurately known and measured properties, than to use one which is formally exact but works with crudely known and derived properties. This is because results from the approximate technique will often have **smaller uncertainties** than those from exact techniques.

Assumptions in Simple Model

$$\dot{v} = a \qquad \text{Eqn 1}$$

$$\dot{z} = -v \qquad \text{Eqn 2}$$

$$a_{n+1/2} = (v_{n+1} - v_n)\frac{1}{\Delta} \qquad \text{Eqn 3}$$

$$v_{n+1/2} = \frac{1}{2}(v_n + v_{n+1}) \qquad \text{Eqn 4}$$

$$z_{n+1/2} = z_n - (v_{n+1} + 3v_n)\frac{\Delta}{8} \qquad \text{Eqn 5}$$

Vertical entry into a non-rotating atmosphere, neglecting gravity, so the only force on the spacecraft is aerodynamic drag. Velocity, v, is known at equally spaced time intervals of Δ from Doppler shifts in the telemetry. Each measurement of v has same random error, σ_v, except for v_0 which is known exactly from cruise tracking. v is positive, so acceleration, a, is negative. First, the trajectory (altitude, z) must be found from the measurements of v. For algebraic convenience, I shall find z at times halfway between each measurement of v. I also derive acceleration, a, and v at these times for later use.

Relationships between atmospheric properties and trajectory

$$\dot{v} = a = -\rho C_D v^2 \quad A/m \qquad \text{Eqn 6}$$

$$p = \int -\rho g z \, . \, dz \qquad \text{Eqn 7}$$

$$\rho k_B T = p M_{mol} \qquad \text{Eqn 8}$$

Eqn 6 relates the atmospheric density, ρ, to the spacecraft's velocity and acceleration. C_D is the drag coefficient, usually close to 2, which is known as a function of v, ρ, and temperature, T. A is the cross-sectional area of the spacecraft, and m is its mass. ρ and pressure, p, are related by hydrostatic equilibrium in Eqn 7. p, ρ, and T are related in the ideal gas law, Eqn 8, using Boltzmann's constant, k_B, and the known mean molecular mass, M_{mol}.

I shall manipulate these three equations in various ways to obtain expressions for ρ, p, and T using a, v, and z with the known C_D, m, A, k_B, and M_{mol}.

First and Only Technique for ρ

$$\rho_{n+1/2} = \frac{v_{n+1} - v_n}{(v_n + v_{n+1})^2} \frac{4m}{\Delta A C_D}$$ Eqn 9

$$\rho_n^2 = \rho_{n+1/2} \rho_{n-1/2}$$ Eqn 10

Starting from Eqn 6, I use Eqns 3 and 4 for a and v and obtain Eqn 9 for ρ. Its use of the small difference between the large and uncertain v_n and v_{n+1} will make this derived density have **large uncertainties**. Hence p and T derived from it may also have large uncertainties... It will also be useful later to know ρ_n, for which I use the geometric mean of $\rho_{n-1/2}$ and $\rho_{n+1/2}$ (Eqn 10).

First Techniques for p and T (Traditional)

$$p_{n+1}^{*} = p_n^{*} + \rho_{n+1/2}\, g\,(z_n - z_{n+1})$$ Eqn 11

$$\rho_n k_B T_n^{*} = p_n^{*} M_{mol}$$ Eqn 12

Starting from Eqn 7, I can use the results from Eqns 5 and 9 for z and ρ to find p*. I label pressures derived by this technique p* to distinguish them from the other derived pressures. Starting from eqn 8, I use the results from eqns 10 and 11 for ρ and p* to find T* in Eqn 12.

Second Techniques for p and T (Isothermal)

$$T^{@} = -M_{mol}\frac{g}{k_B}\frac{dz}{d(\ln \rho)}$$ Eqn 13

$$T_n^{@} = -M_{mol}\frac{g}{k_B}\frac{z_{n+1/2} - z_{n-1/2}}{\ln \rho_{n+1/2} - \ln \rho_{n-1/2}}$$ Eqn 14

$$\rho_n k_B T_n^{@} = p_n^{@} M_{mol}$$ Eqn 15

Combining the assumption of an **isothermal atmosphere** with Eqns 7 and 8 gives Eqn 13 above. $z_{n+1/2}$ and $\rho_{n+1/2}$, from Eqns 5 and 9, can be used to find $T^{@}$ and then $p^{@}$ in Eqns 14 and 15.

Special Case at Peak Deceleration

$$T_n^{\#} = \frac{M_{mol}\, g\, \Delta}{k_B} \frac{v_n^2}{(v_{n-1} - v_{n+1})}$$

Eqn 16

The formula for $T^{@}$ in terms of the measured velocities (not shown) can be **simplified greatly at peak deceleration** when $v_{n-1} = v_n + \delta$ and $v_{n+1} = v_n - \delta$. This result for $T^{@}$ at peak deceleration, which I call $T^{\#}$, is shown above. It is only valid at peak deceleration and is useless everywhere else.

Third Techniques for p and T (Constant C_D and Isothermal)

$$\int \frac{dv}{v} = \frac{A}{mg} \int \rho \, g \, C_D \, . \, dz = \frac{-C_D A}{mg} \int dp^{\$} \qquad \text{Eqn 17}$$

$$p_n^{\$} - p_0 = \frac{-mg}{C_D A} \ln \left(\frac{v_n}{v_0} \right) \qquad \text{Eqn 18}$$

$$T^{\$} = - M_{mol} \frac{g}{k_B} \frac{dz}{d \left(\ln p^{\$} \right)} \qquad \text{Eqn 19}$$

$$T^{\$}_{n+1/2} = - M_{mol} \frac{g}{k_B} \frac{z_n - z_{n-1}}{\ln p_{n+1} - \ln p_n} \qquad \text{Eqn 20}$$

Dividing Eqn 6 by Eqn 2 and rearranging gives Eqn 17. Assuming that **C_D is constant** leads to Eqn 18. p_0, which is negligibly small, and v_0, which is well-known from cruise tracking, are the top of the atmosphere values. The assumption of constant C_D is accurate to about 20% or so, perfectly adequate for studying pressures which vary by many orders of magnitude. Again assuming an **isothermal atmosphere** leads to Eqns 19 and 20.

Summary of Different Techniques

The first and only technique for density depends on the small difference between two large and poorly known velocities, so has large uncertainties. The first techniques for pressure (p*) and temperature (T*) rely on integrating these densities with respect to altitude, which gives uncertain results but does not make any additional simplifying assumptions. The second techniques for pressure ($p^{@}$) and temperature ($T^{@}$) assume an isothermal atmosphere and also rely on ratios of derived densities, which will be very uncertain indeed. The special case of peak deceleration in the $T^{@}$ technique leads to a temperature estimate ($T^{\#}$) which has small uncertainties. The third techniques for pressure ($p^{\$}$) and temperature ($T^{\$}$) assume that C_D is constant and do not rely on differences between velocities, hence they should have small uncertainties

Application of these Techniques to a Pathfinder-like Entry

Error in derived velocity, v, is predominantly due to **uncertainty in transmission frequency** of spacecraft, $\sigma_v = c\ \sigma_{trans} / f_{trans}$. Pathfinder's transmitter had a systematic drift with maximum drift value of 10^{-7} of the nominal frequency (8 GHz), but I will assume random errors with $\sigma_{trans} / f_{trans}$ of 10^{-7} . This makes the error analysis easier. I choose m=500 kg, A=5 m^2, a vertical entry speed of 2 km s^{-1} at 120 km, $C_D = 2$, and an isothermal atmosphere at 200 K with a surface density of 10^{-2} kg m^{-3}.

I first derive the actual entry trajectory under these conditions and extract v at every 4 seconds. Next I add random errors to these values of v corresponding to the noise level discussed above, and use these noisy v values with my various techniques to derive the trajectory and atmospheric structure. These derived results are then compared to the actual values specified for the simulated entry. The uncertainty analysis is not presented here, but can be found in my dissertation.

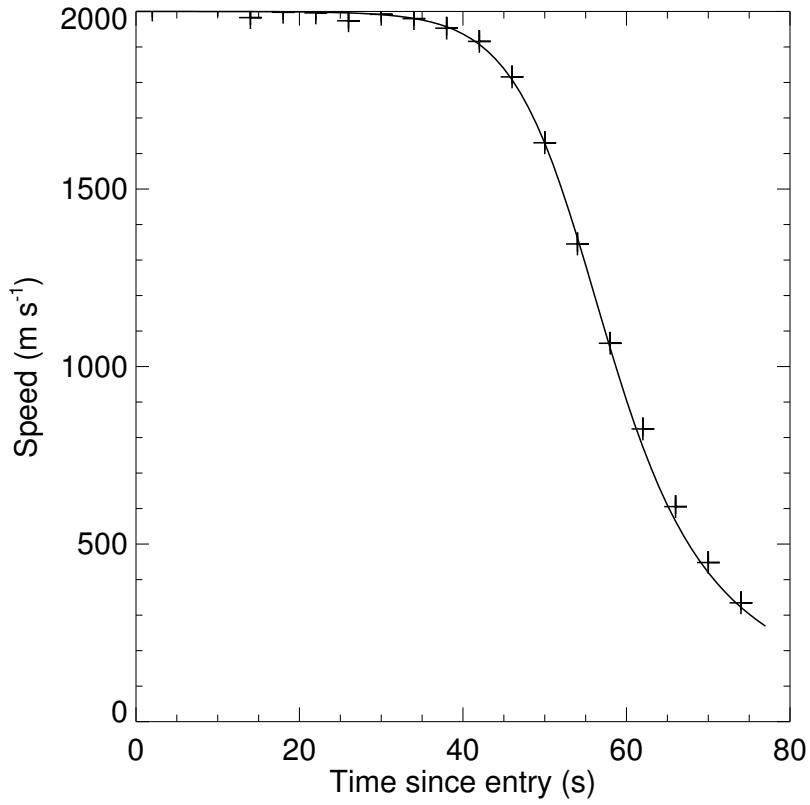

Fig 1. $v_{n+1/2}$ (crosses) and uncertainties (vertical lines) versus time since entry, derived using the noisy values of v from Doppler measurements. The continuous curve shows the speeds that actually occurred in the simulated entry.

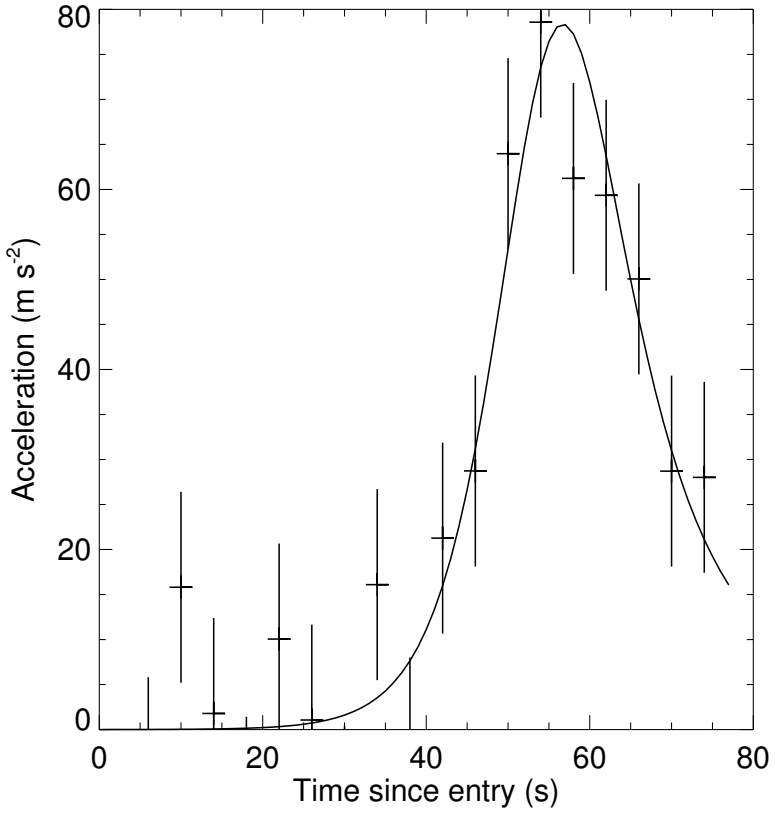

Fig 2. $a_{n+1/2}$ (crosses) and uncertainties (vertical lines) versus time since entry, derived using the noisy values of v from Doppler measurements. The continuous curve shows the accelerations that actually occurred in the simulated entry.

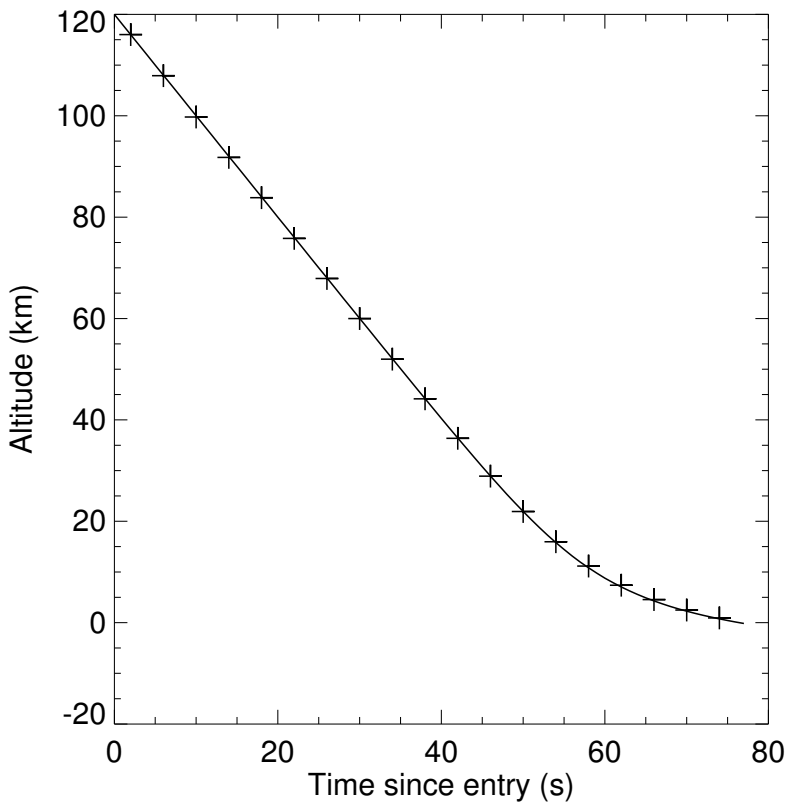

Fig 3. $z_{n+1/2}$ (crosses) and uncertainties (vertical lines) versus time since entry, derived using the noisy values of v from Doppler measurements. The continuous curve shows the altitudes that actually occurred in the simulated entry.

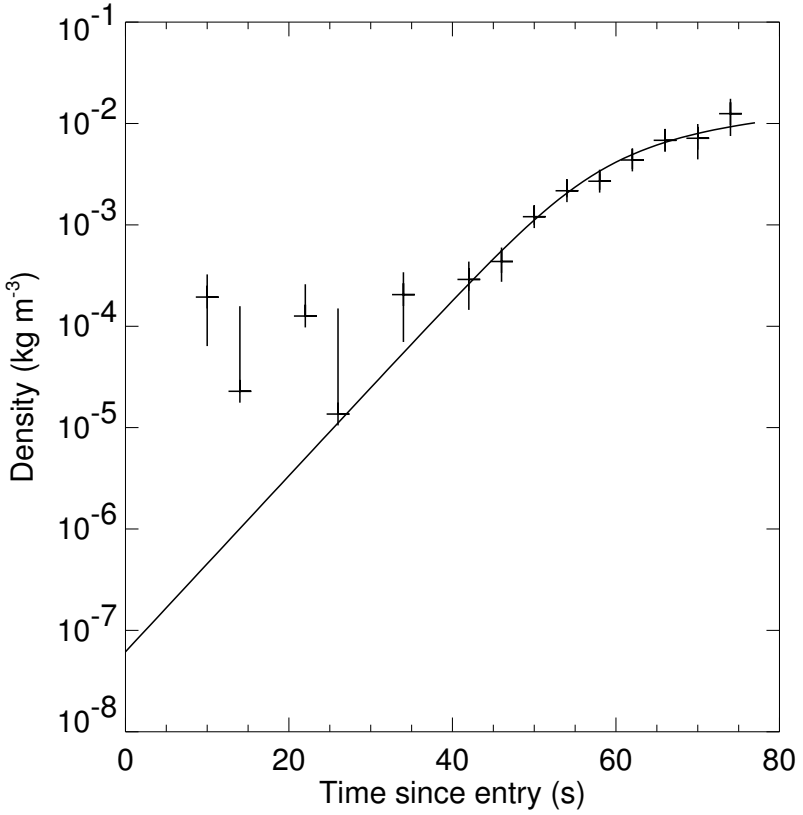

Fig 4. **First and only technique for density.**

$\rho_{n+1/2}$ (crosses) and uncertainties (vertical lines) versus time since entry, derived using the noisy values of v from Doppler measurements. If the uncertainty is greater than the nominal value, then only one side of the error bar is plotted. The continuous curve shows the densities that actually occurred in the simulated entry.

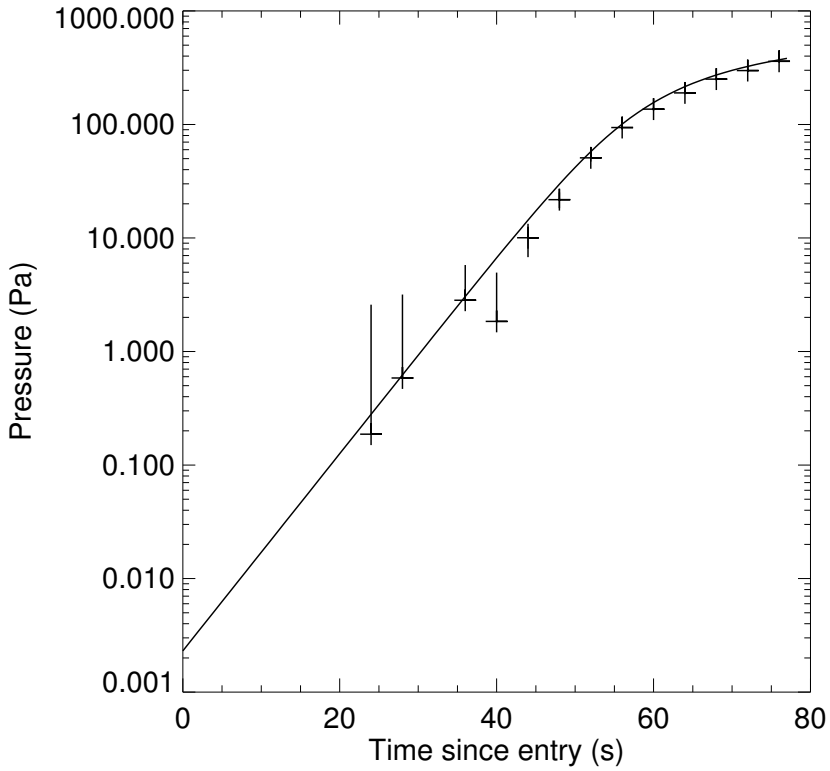

Fig 5. **First technique for pressure.**
p^*_n (crosses) and uncertainties (vertical lines) versus time since entry, derived using the noisy values of v from Doppler measurements. If the uncertainty is greater than the nominal value, then only one side of the error bar is plotted. The continuous curve shows the pressures that actually occurred in the simulated entry.

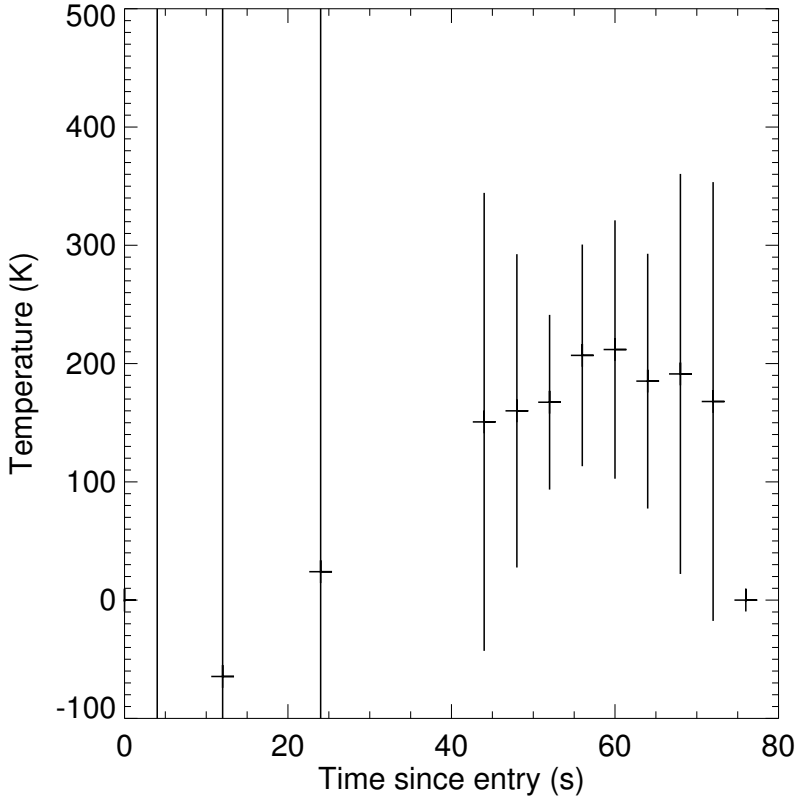

Fig 6. **First technique for temperature.**
T^*_n (crosses) and uncertainties (vertical lines) versus time since entry, derived using the noisy values of v from Doppler measurements. If the uncertainty is greater than the nominal value, then only one side of the error bar is plotted. The continuous curve shows the temperatures that actually occurred in the simulated entry.

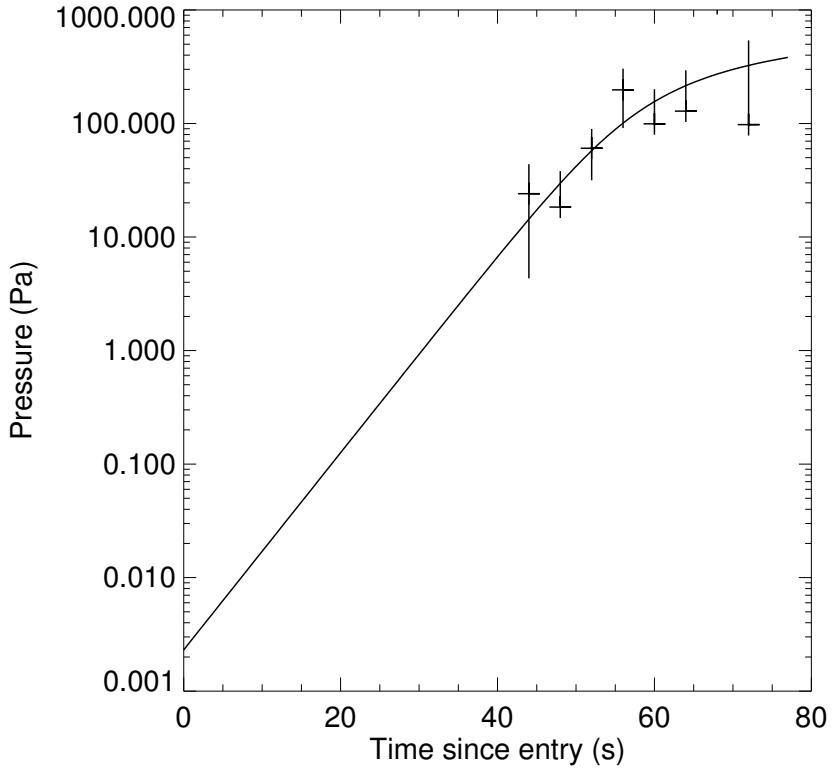

Fig 7. **Second technique for pressure.** $p^{@}_{n}$ (crosses) and uncertainties (vertical lines) versus time since entry, derived using the noisy values of v from Doppler measurements. If the uncertainty is greater than the nominal value, then only one side of the error bar is plotted. The continuous curve shows the pressures that actually occurred in the simulated entry.

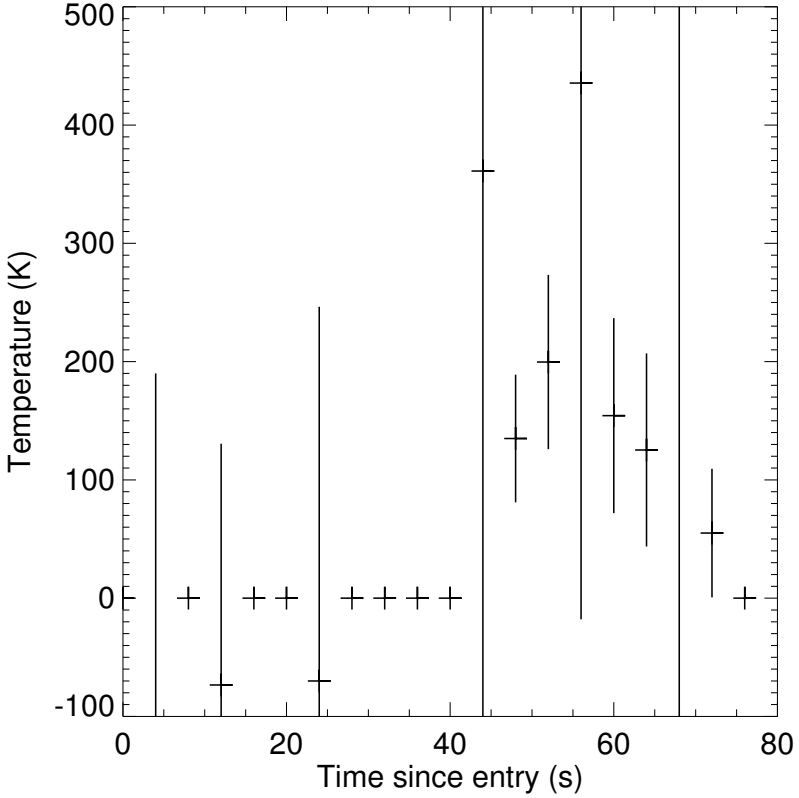

Fig 8. **Second technique for temperature.** $T^{@}_{n}$ (crosses) and uncertainties (vertical lines) versus time since entry, derived using the noisy values of v from Doppler measurements. If the uncertainty is greater than the nominal value, then only one side of the error bar is plotted. The continuous curve shows the temperatures that actually occurred in the simulated entry.

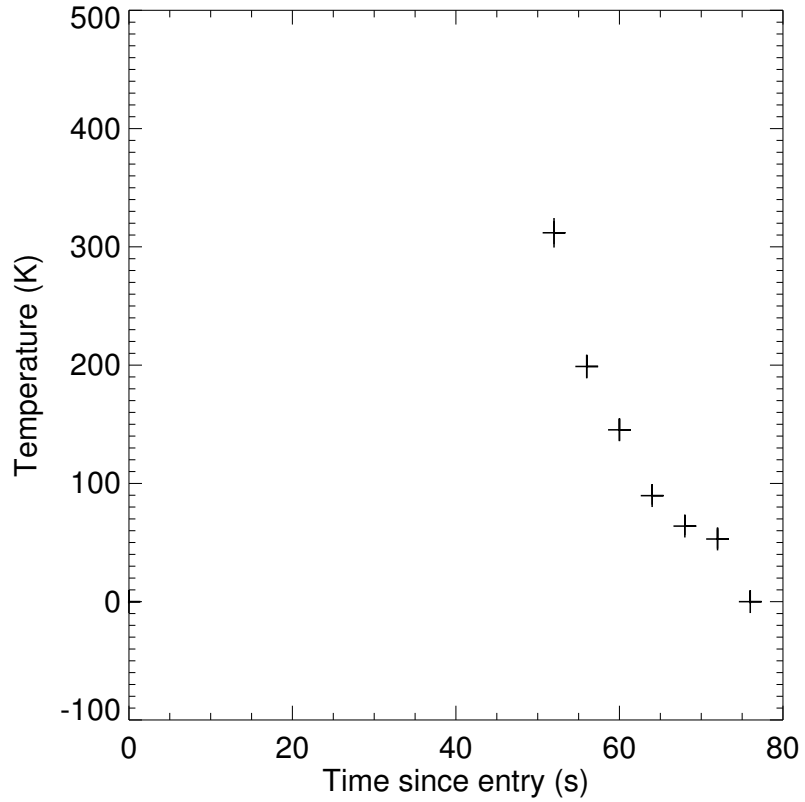

Fig 9. **Special case of Second technique for temperature at peak deceleration.** $T^{\#}_{n}$ (crosses) and uncertainties (vertical lines) versus time since entry, derived using the noisy values of v from Doppler measurements. If the uncertainty is greater than the nominal value, then only one side of the error bar is plotted. The continuous curve shows the temperatures that actually occurred in the simulated entry. The only derived temperature on this figure that is useful is that which occurs at peak deceleration, or 54s using an earlier figure. $T^{\#}_{54s}$ is close to the specified value of 200K.

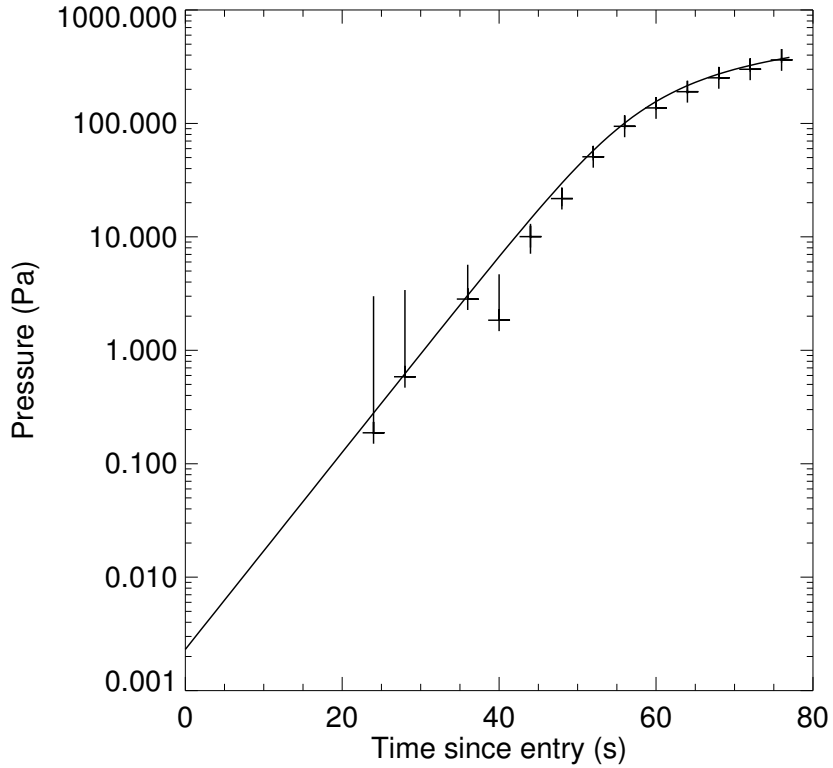

Fig 10. **Third technique for pressure.** $p^{\#}_{n}$ (crosses) and uncertainties (vertical lines) versus time since entry, derived using the noisy values of v from Doppler measurements. If the uncertainty is greater than the nominal value, then only one side of the error bar is plotted. The continuous curve shows the pressures that actually occurred in the simulated entry.

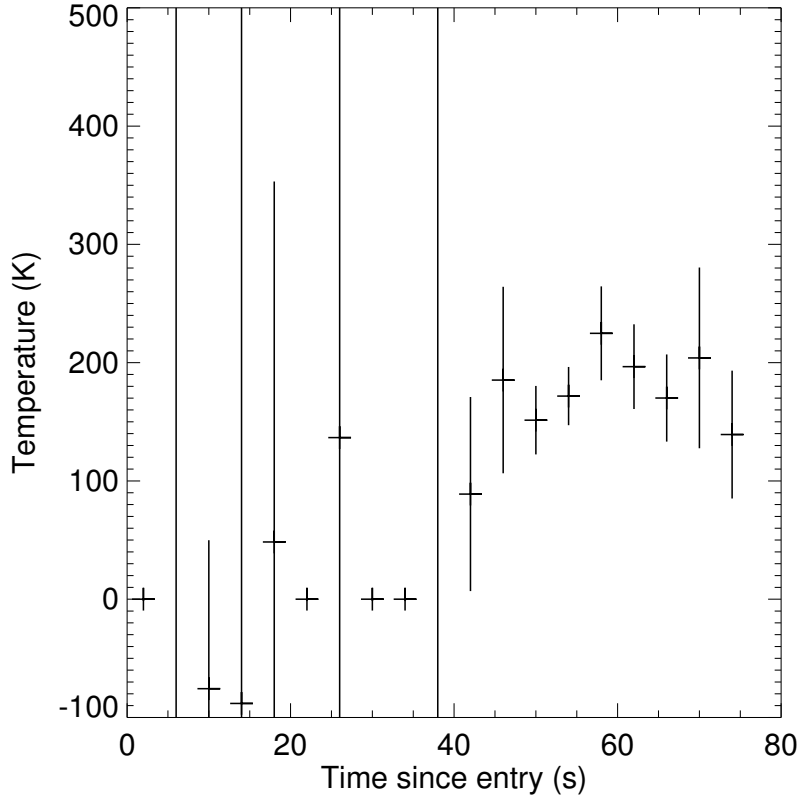

Fig 11. **Third technique for temperature.** $T^{\#}_{n+1/2}$ (crosses) and uncertainties (vertical lines) versus time since entry, derived using the noisy values of v from Doppler measurements. If the uncertainty is greater than the nominal value, then only one side of the error bar is plotted. The continuous curve shows the temperatures that actually occurred in the simulated entry.

Discussion of Figures

The derived altitudes (Fig 3) and velocities (Fig 1) are accurate, but the derived accelerations (Fig 2) are, as expected, much less accurate.

The derived densities (Fig 4) are only useful in the lower atmosphere.

Both the first and third techniques for pressure (Figs 5 and 10) give useful results in the lower atmosphere, but the second technique for pressure (Fig 7) is near useless.

The first and third techniques for temperature (Figs 6 and 11) give noisy results that, in the lower atmosphere, are scattered around the true value. Averaging within these would give a better temperature result, but with lower vertical resolution.

The second technique for temperature (Fig 8) is near useless, but its special case at peak deceleration (Fig 9) appears to give one, and only one, very accurate temperature measurement.

Conclusions

Atmospheric properties derived by any of these techniques will have such large uncertainties that they are only likely to be scientifically useful on a planet whose atmosphere has not be studied be entry accelerometers before. They might be useful for other reasons if there is programmatic or public interest either in immediate results during a successful entry or in results from an unsuccessful entry.

The assumptions of random noise, rather than systematic drift, and of a constant C_D or isothermal atmosphere will introduce some bias and additional uncertainties into the derived atmospheric properties. Using accurate entry geometry and including gravity will make the techniques more complicated, but are not too difficult. I hope to test these techniques on the successful entries of MER-A and MER-B. If validated, they can be used for operational support of Phoenix and MSL.

I acknowledge helpful discussions of Mars Pathfinder with Sam Thurman at JPL.

See also Chapter 6 of http://www.lpl.arizona.edu/~withers/phd.html